

Orientation-resolved $3d_{5/2}$ binding energy shift of Rh and Pd surfaces: anisotropy of the skin-depth lattice strain and quantum trapping

Yan Wang,^a Yan Guang Nie,^b Ji Sheng Pan,^c L. K. Pan,^d Zhuo Sun,^d
Ling Ling Wang^a and Chang Q. Sun^{*be}

Received 22nd August 2009, Accepted 17th December 2009

First published as an Advance Article on the web 18th January 2010

DOI: 10.1039/b917326a

Incorporating the BOLS correlation algorithm [Y. Sun, *J. Phys. Chem. C*, 2009, **113**, 14696] into high-resolution XPS measurements [J. N. Andersen, *et al.*, *Phys. Rev. B: Condens. Matter*, 1994, **50**, 17525; A. Baraldi, *et al.*, *New J. Phys.*, 2007, **9**, 143] has produced an effective way of determining the $3d_{5/2}$ energy levels of isolated Rh(302.163 ± 0.003 eV) and Pd (330.261 ± 0.004 eV) atoms and their respective bulk shifts (4.367 and 4.359 eV) with a refinement of the effective atomic coordination numbers of the top (100), (110), and (111) atomic layers (4.00, 3.87, and 4.26, respectively). It is further confirmed that the shorter and stronger bonds between under-coordinated atoms induce local strain and skin-depth charge-and-energy quantum trapping and, hence, dictate globally the positive core level binding energy shifts.

I. Introduction

Unlike the valence density-of-states (DOS), which provides direct information about charge transportation and polarization upon a chemical reaction taking place,^{1,2} the energy shift of the core-level of an isolated atom upon bulk, surface, or nanostructure formation gives profound information about the crystal binding energy (BE), which is dominated by interatomic interaction.^{3,4} Spontaneous processes such as alteration of the bond nature and relaxation of the bond length will affect the crystal field and hence shift the core-level BE intrinsically towards lower (large absolute value) BE values to a certain extent. It has been verified that the BE shift is proportional to the equilibrium cohesive energy per bond.⁵ Being able to discriminate the crystal binding (core-level shift) from intraatomic trapping (core-level position of an isolated atom) of a core electron under various physical and chemical environments is a great challenge, which is beyond the scope of direct measurement using currently available probing technologies such X-ray photoelectron spectroscopy (XPS). Combining the most advanced laser cooling technology and XPS, one can measure the energy separation between different energy levels of the slow-moving gaseous atoms trapped by the laser beams but, up to now, the individual core-level energy of a statically isolated atom cannot be obtained.⁶ What one can

measure using XPS are the convoluted broad peaks of the core-bands contributing from intraatomic trapping, crystal binding, crystal orientation, surface relaxation, nanosolid formation, and surface passivation.

In addition to the well-known chemical shift caused by the core-hole 'screening' due to charge transportation in a reaction, relaxed atomic layers at a surface can split the core-band of a specimen into a few components. However, the energy assignment of the components induced by surface relaxation is quite controversial, due to the lack of constraints for assigning which peak arises from the surface and which one is from the bulk, and what is the separation between them.⁵ With the widely used sign convention, a positive shift relates the low-energy component to the surface (S_i , $i = 1, 2, \dots, B$) while the high-energy component to the bulk (B), and *vice versa*. The resultant peak is often located in between the components and the exact position of the resultant peak varies with crystal orientation, surface finish and experimental conditions such as the incident beam energy and the taking-off angles between the beam and the surface normal. Generally, the assignment of a surface positive core-band shift is favoured because XPS measurements^{7–16} revealed that the intensity of the low-energy (B) component often increases with the incident beam energy or when decreasing the angle between the incident beam and the surface normal in the measurement.

Dominated by the under-coordinated atoms, the XPS core-band features (both the main peak and the chemical satellites) of nanostructures move simultaneously towards lower BE and the amount of shift depends on both the original core-level energies of the components and the shape and size of the particle. It has been confirmed using XPS that size-reduction induces a positive core level shift of Ni,^{17,18} Pt,^{19–26} Au,^{27–29} Cu,³⁰ Pd,³¹ and Si nanostructures,³² and coordination-reduction also causes the C 1s BE of carbon allotropes to shift positively.^{33–35} Compared with the mono-peak of S-2p and S-2s core bands of ZnS and CdS bulks, the S-2p and S-2s bands of both ZnS and CdS nanosolids exhibit three

^a School of Physics and Microelectronics Science, Hunan University, Changsha 410082, China

^b School of Electrical and Electronic Engineering, Nanyang Technological University, Singapore 639798. E-mail: Ecqsun@ntu.edu.sg

^c Institute of Materials Research and Engineering, Agency for Science, Technology and Research (A*STAR), Singapore 117602

^d Engineering Research Center for Nanophotonics & Advanced Instrument, Ministry of Education, Department of Physics, East China Normal University, Shanghai 200062, China

^e Faculty of Materials, Optoelectronics and Physical Science and Key Laboratory of Low-Dimensional Materials and Application Technologies (Xiangtan University), Ministry of Education, Changsha 411105, China

components.³⁶ These components have been ascribed to the contribution, from low to high BE, from the outermost capping and the subsequent surface layers that are one atomic diameter thick, and the core interior of the nanosolid. The size trend of the core level shift is in accordance with the surface positive shift. It has been shown³⁷ that the inverse-size dependence of the physical properties of nanostructures arise from only a limited number of the outermost atomic layers instead of the entire solid. Therefore, as physical origin, surface relaxation and nanosolid formation play the equivalent role in splitting and shifting the core-levels of a specimen.

However, development of an approach extracting quantitative information regarding the energetic behavior of core electrons from photoelectron measurements of the surface core level variation has long been a challenge, though the surface- and size-induced core level shifts of materials have been extensively investigated. The major challenge includes: (i) clarification of the shift direction of the surface components; (ii) determination of the energy levels of an isolated atom and their bulk shifts, which should not be zero; (iii) energy correlation between the atomic-layer and crystal-orientation resolved components; (iv) mechanism behind these energy shifts; and, (iv) further information one can learn from the XPS measurement.

The objective of this work is to show that an incorporation of the bond order–length–strength (BOLS) correlation algorithm^{3,38} and tight binding theory² into the well-measured sets of high-resolution XPS data^{12,39} enabled us to determine the 3d_{5/2} energy levels of the isolated Rh and Pd atoms and their respective bulk shift with a refinement of the effective atomic coordination numbers (CN) of the fcc(100), (110), and (111) atomic layers. Based on this understanding, we are able to gain information about the local strain, the relative binding energy density and the atomic cohesive energy in the surface skin. It is evidenced further that the shorter and stronger bonds between under-coordinated atoms and the associated skin-depth charge and energy quantum trapping are responsible for the positive surface core level shifts.

II. Principle

The BOLS correlation mechanism³⁸ indicates that the remaining bonds of an under-coordinated atom contract and strengthen spontaneously, leading to the formation of local strain and quantum trapping, and also the densification of charge and energy at local sites around atomic defects, adatoms, surfaces, grain boundaries, dislocations, terrace edges, dimers, atomic chains, atomic sheets, hollow tubes, or the skins of nanostructures and nanocavities.³ The development of this strain-induced quantum trapping forms a perturbation to the Hamiltonian of the originally extended structure due to the unusual boundary conditions. With this physical picture of atomic CN imperfection as the basis, the BOLS can account for the size-induced core level shifts, band gap expansion, solid–liquid transition, and surface and nanostructure mechanical strength. Furthermore, the ability of the BOLS to calculate the energy levels of an isolated atom and the energy shift of the bulk sample with great sensitivity, *i.e.* to make the distinction between the effects of the interatomic binding *versus* the intra-atomic trapping potential on the

electron, has not yet been achieved by other theoretical methods. This can be done *via* two routes—either based on XPS measurements of the BEs of samples of varying dimensions (size effect), or from the decomposition of a single BE peak spectrum from a well defined surface (surface effect).

According to the energy band theory² and the BOLS correlation, the Hamiltonian of the crystal undergoes the perturbation Δ_H due to the atomic CN deficiency experienced by surface atoms and those in adjacent layers to the crystal potential, $V_{\text{cryst}}(r)$, while the intra-atomic trapping, $V_{\text{atom}}(r)$, remains unchangeable,

$$V(\Delta_i) = V_{\text{atom}}(r) + V_{\text{cryst}}(r)[1 + \Delta_i]$$

Where, the $\Delta_i = c_i^{-m} - 1$ represents the perturbation to the Hamiltonian experienced by the core electrons of an atom in the i th surface layer, which follows the relationships between the atomic CN (z_i), bond length (d_i) and bond energy (E_i):

$$\begin{cases} c_i = d_i/d_b = 2/[1 + \exp(12 - z_i)/8z_i] \\ E_i = c_i^{-m} E_b \end{cases} \quad (1)$$

The c_i is the bond contraction coefficient, which is dependent on the coordination of the atom, z_i for all kinds of chemical bonds. Subscript b represents the bulk values. The z_1 ($i = 1$) should vary slightly with crystal orientation but confirmation of this has been impossible up to now. Intuitively, one often takes $z_1 = 6$ for an fcc structure but available data favors the effective z_1 value of 4 (with $c_i \sim 12\%$) or thereabouts.^{7,11,38} For Nb(001)-3d_{3/2} example, the first layer spacing contracts by 12% in association with the 0.50 eV core-level shift.⁷ A $(10 \pm 3)\%$ contraction of the first layer spacing has caused the Ta(001)-4f_{5/2(7/2)} level to shift by 0.75 eV.¹¹ The positive surface core-level shift of Nb-3d and Ta-4f has been attributed to the enhancement of the interlayer charge density and the enhancement of the resonant diffraction of the incident irradiation due to the surface bond contraction.^{7,11,38}

Also, the magnitude of a remaining bond's BE of an under-coordinated surface atom (E_i) increases as the bonds contract spontaneously, and is equal to the “ c_i^{-m} ” times of the energy of a single bond in a bulk sample (E_b). The parameter m , which is not freely adjustable, characterizes the nature of a bond in a solid, or otherwise deciphered as the parameter relating the bond energy to its length. For pure metal, m has been optimized as one.³⁸

Incorporating the BOLS correlation into the band theory with the surface-induced Hamiltonian perturbation, the energy shift of a specific ν th energy level of an atom in the surface layer with respect to that of an isolated atom is:

$$\begin{aligned} \Delta E_{\nu}(i) &= E_{\nu}(i) - E_{\nu}(0) = \Delta E_{\nu}(\mathbf{B})(1 + \Delta_H) \\ &= [E_{\nu}(\mathbf{B}) - E_{\nu}(0)](1 + \Delta_H) \end{aligned}$$

Where,

$$\begin{cases} E_{\nu}(0) = \langle \phi_{\nu}(r) | V_{\text{atom}}(r) | \phi_{\nu}(r) \rangle & \text{(Core level energy)} \\ \Delta E_{\nu}(\mathbf{B}) = \beta + z\gamma \propto \langle E_b \rangle & \text{(Core level shift)} \\ \beta = \langle \phi_{\nu}(r) | V_{\text{cry}}(r) | \phi_{\nu}(r) \rangle \propto \langle E_b \rangle & \text{(Exchange integral)} \\ \gamma = \langle \phi_{\nu}(r) | V_{\text{cry}}(r) | \phi_{\nu}(r') \rangle \propto \langle E_b \rangle & \text{(Overlap integral)} \end{cases} \quad (2)$$

The intra-atomic trapping potential, $V_{\text{atom}}(r)$, determines the ν th energy level of an isolated atom, $E_\nu(0)$. The $\phi_\nu(r) = (r \neq r')$ is the specific Bloch wave function at site r . The parameter z is the weighting factor of the overlapping integral contribution to the $E_\nu(\mathbf{B})$. Because of the strong localization nature of the core electrons, the overlapping integral is negligibly small compared with the exchange integral. Therefore, the interatomic bond energy, $\langle E_b \rangle$, dominates the shift of BE. Eqn (2) can be reorganized as:

$$\frac{E_\nu(i) - E_\nu(0)}{E_\nu(\mathbf{B}) - E_\nu(0)} = c_i^{-1} = 1 + \Delta_i \text{ or,} \quad (3)$$

$$\frac{E_\nu(K) - E_\nu(\mathbf{B})}{E_\nu(\mathbf{B}) - E_\nu(0)} = \Delta_i$$

Therefore, only the under-coordinated atoms in the surface skin contribute the perturbation Δ_H to the overall Hamiltonian. The core level shift caused by bond order loss is thus shown to be positive.

A recent XPS study⁴⁰ confirmed that the Ni 2p levels of the outermost three atomic layers shift positively to lower BE discretely, with the outermost atomic layer shifting the most. From the electronic structure point of view, the surface of transition and noble metals consists of at most three atomic layers or two interatomic spacings.^{41,42}

For the surface positive BE shift, we have the constraint for the relative shift of each surface component,

$$\frac{E_\nu(i) - E_\nu(0)}{E_\nu(i') - E_\nu(0)} = \frac{c_{i'}}{c_i} \text{, or} \quad (4)$$

$$\frac{E_\nu(i) - E_\nu(\mathbf{B})}{E_\nu(i') - E_\nu(\mathbf{B})} = \frac{c_{i'} - 1}{c_i - 1} \text{, } (i = S_1, S_2, \mathbf{B}; i' \neq i)$$

which yields,

$$\left\{ \begin{aligned} E_\nu(0) &= \frac{c_i^{-1} E_\nu(i) - c_i^{-1} E_\nu(i')}{c_i^{-1} - c_i'^{-1}} = \frac{c_i E_\nu(i) - c_i' E_\nu(i')}{c_i - c_i'} \\ \Delta E_\nu(\mathbf{B}) &= [E_\nu(i) - E_\nu(0)] c_i \end{aligned} \right. \quad (5)$$

Using eqn (5), we can readily determine the energy level $E_\nu(0)$ of an isolated atom and its bulk shift $\Delta E_\nu(\mathbf{B})$ and the effective CNs of the first layer at different orientations through analyzing the measurements of surface induced positive core-level shift.

Based on the BOLS derivatives, we can also predict the coordination-resolved relative atomic cohesive energy ($E_c = E_c(z_i)/E_c(\mathbf{B}) = z_i E_i / z_b E_b = z_{ib} c_i^{-1}$), and the binding energy density ($E_d = [E_d(z_i)/d_i^3] / [E_d(z_b)/d_b^3] = c_i^{-4}$) at atomic sites in the outermost three planes.³ Therefore, from the XPS data we can obtain comprehensive information regarding the bond order, length, energy, the atomic cohesive energy and the binding energy density (z_i , d_i , E_i , E_c , and E_d). These quantities are intrinsic factors dominating the performance and process at a surface such as growth nucleation and chemical reaction. For example, the energy density determines the local elasticity and the atomic cohesive energy dictates the critical temperature of phase transition.³⁸

Fig. 1 illustrates the BOLS-derived BE shift of surface component layers. $E_\nu(0)$ is the energy level of an isolated atom, from which the core level shifts. S_1 ($z_1 \cong 4$ ^{7,11,38}) and S_2 correspond to the top and the second atomic layer and \mathbf{B}

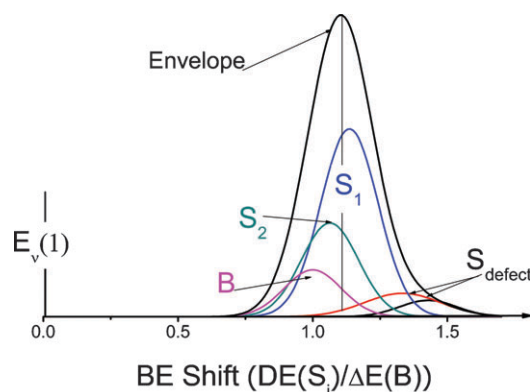


Fig. 1 Illustration of the XPS spectrum. $E(1)$ is the energy level of an isolated atom, which is the reference for the shifts of other components that follows these constraints: (1) there should be components representing the \mathbf{B} , S_2 , S_1 and S_{defect} ; (2) the energy shift should be positive and the low- z components shift further; (3) the energy shift of each component is proportional to the magnitude of bond energy, which follows this relation: $\Delta E_\nu(i) : \Delta E_\nu(\mathbf{B}) = E_i : E_b = c_i^{-m}$ ($i = S_{\text{defect}}, S_1, S_2$).

the bulk components. S_{defect} ($z < 4$) represents the adatoms or edge atoms with even lower atomic CNs. The intensities of the components are subject to the fraction of the specifically z -coordinated atoms, which is constrained by the measured intensity of the spectrum. The energy values of the peaks satisfy the criterion: $\Delta E_\nu(i) : \Delta E_\nu(\mathbf{B}) = E_i : E_b = c_i^{-1}$, according to eqn (4). For a surface, the peak energies of the components may fluctuate slightly with varying experimental conditions such as temperature, crystal orientation, and incident radiation beam angle,⁵ but the $E_\nu(0)$ and its bulk shift $\Delta E_\nu(\mathbf{B})$ will not change for a given specimen.

From the above discussions, we can establish the rules for XPS surface spectral decomposition:

1. There should be 3 or 4 components representing the \mathbf{B} , S_2 , S_1 and S_{defect} contributions for transition and noble metals.^{40,41} For lighter atoms, or polarized systems, the number of peaks may increase.
2. For each specimen, the $E_\nu(0)$ and its bulk shift (\mathbf{B} component) are not changeable under any circumstances as they are intrinsic constants.
3. The energy shift should be positive and the low- z components shift further (eqn (4)). The energy shift of each component is proportional to the magnitude of bond energy, which follows this relation: $\Delta E_\nu(i) : \Delta E_\nu(\mathbf{B}) = E_i : E_b = c_i^{-1}$ ($i = S_{\text{defect}}, S_1, S_2$).
4. The resultant intensity of the components is constrained by the measured spectral intensity. The width and intensity of each component in the initial decomposition^{12,39} for the particular Rh and Pd examples were taken as references for fine tuning under constraint 4.
5. The neighboring Rh($5s^1 4d^8$) and Pd($4d^{10}$) noble metals in the Periodic table share the same fcc structure; the effective CNs of the Rh and Pd surfaces of the same orientation should be identical. This adds another constraint for atomic CN refinement.
6. If a total of l components are involved in decomposing a set of XPS spectra from the different orientations of the same specimen, the $E_\nu(0)$ should take the mean value of $N = C_l^2 = l! / [(l-2)!2!]$ possible combinations with a

standard deviation σ . The minimal standard deviation serves as a criterion for the accuracy of spectral decomposition.

With the above constraints, we are able to determine the atomic-layer and crystal-orientation resolved effective CN, local strain, quantum trap depth, the 3d energy level of an isolated Pd and Rh atom and their bulk shift, as well as the ratio of binding energy density and the atomic cohesive energy, which are beyond the scope of available methods. However, the combination of BOLS and tight binding theory is unable to determine the absolute intensity and width of each component as they are more dependant on experimental conditions.

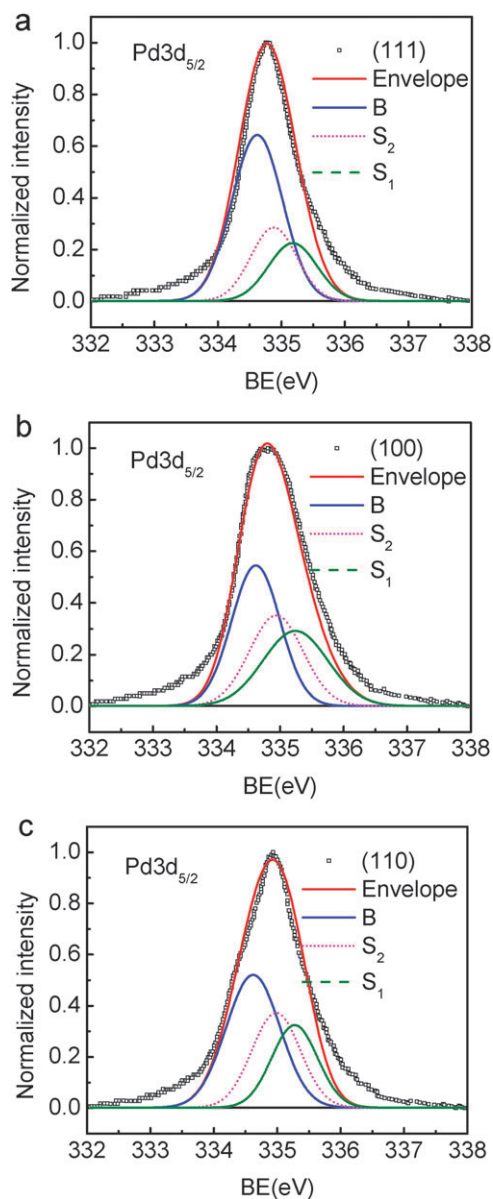


Fig. 2 Decompositions of Pd $3d_{5/2}$ core level spectra¹² for (a) (111), (b) (100) and (c) (110) surfaces with three decomposition Gaussian components S_1 , S_2 and B using the parameters given in Table 1. The XPS spectra were collected with an incident beam energy of 380 eV at normal emission.

III. Results and discussion

Using high-resolution XPS, Anderson *et al.*¹² measured systematically the orientation-resolved $3d_{5/2}$ spectra of the (111), (110) and (100) surfaces of Pd at a photon energy of 390 eV. Using *ab initio* calculations based on the final-initial states model, they suggested that the surface induces negative shifts that vary from 0.25 to 0.60 eV, depending on the orientations and materials. Baraldi *et al.*³⁹ recently measured the Rh surface core level shift at a photon energy of 380 eV and with polar emission angles varying from 20 to 50° with respect to the surface normal. Results showed that the smaller

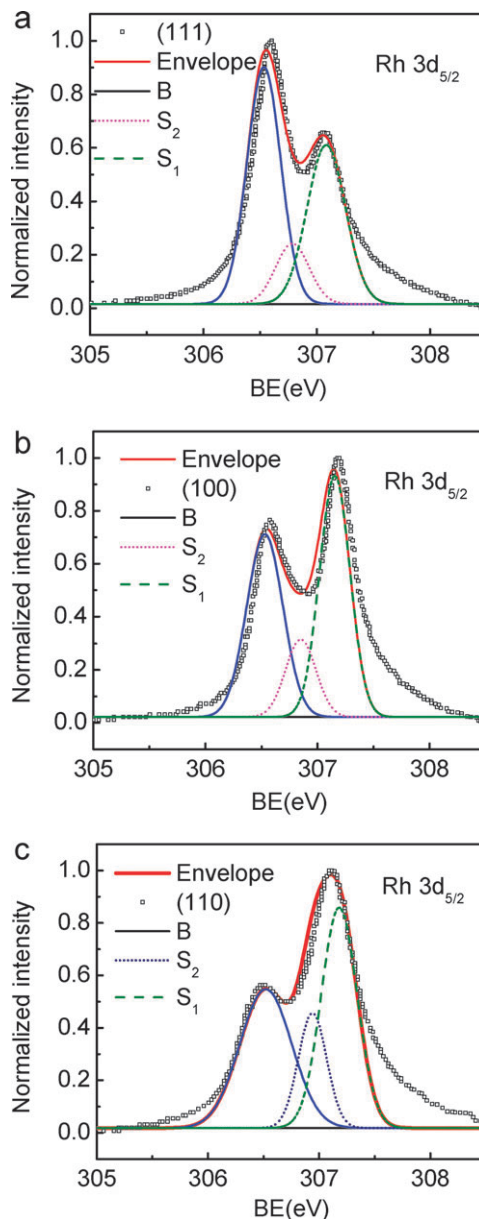


Fig. 3 Decompositions of Rh $3d_{5/2}$ core level spectra for (a) (111),³⁹ (b) (100),³⁹ and (c) (110)¹² with decomposition parameters given in Table 1. The XPS spectra were collected with incident beam energy of 380 eV at normal emission. The asymmetric tails at the lower end of the spectra indicate the presence of defects such as adatoms to the Rh surfaces.

Table 1 Decomposition parameters of the XPS $3d_{5/2}$ core level shift of Rh and Pd surfaces after the Tougaard background is subtracted. The three decomposition Gaussian components, denoted as S_1 , S_2 and B, satisfy the BOLS expectation. The refinement of the orientation-resolved effective CNs arises from the atomic density of each face. The intensity of each component is given for the best fit. Results show the anisotropy of the local lattice strain ($c_i - 1$), relative atomic cohesive energy ($E_c = E_c(z)/E_c(12) = z/c_z/12$), and binding energy density ($E_d = E_d(z)/E_d(12) = c_z^{-4}$) in the three planes. The coordination-resolved $3d_{5/2}$ core level shift for Rh and Pd is expressed as:

$$E_\nu(i) = \langle E_{3d}(0) \rangle (\pm\sigma) + \Delta E_{3d}(B) c_z^{-1} \text{ (eV)}$$

$$= \begin{cases} 302.163(\pm 0.003) + 4.367 c_z^{-1} & \text{(Rh } 3d_{5/2}) \\ 330.261(\pm 0.004) + 4.359 c_z^{-1} & \text{(Pd } 3d_{5/2}) \end{cases} \text{ (eV)}$$

Plane	i	Pd $3d_{5/2}$ [ref. 12]				Rh $3d_{5/2}$ [ref. 39]				$\langle z \rangle$	$c_i - 1$ (%)	E_d	E_c
		$E_{3d}(i)$	I	W	z_i	$E_{3d}(i)$	W	I	z_i				
(111)	B	334.62	0.65	0.95	12	306.53	0.35	0.96	12	12	0.00	1.00	1.00
	S_2	334.88	0.28	0.85	6.31	306.79	0.35	0.24	6.31	6.31	-5.63	1.26	0.56
	S_1	335.18	0.23	0.90	4.24	307.08	0.40	0.61	4.29	4.26	-11.31	1.62	0.40
(100)	B		0.55	0.90			0.38	0.72					
	S_2	334.94	0.36	1.00	5.73	306.85	0.32	0.32	5.73	5.73	-6.83	1.33	0.51
	S_1	335.24	0.30	1.20	4.00	307.15	0.32	0.93	4.00	4.00	-12.44	1.70	0.38
(110)	B		0.52	1.00			0.55	0.54					
	S_2	334.98	0.37	0.90	5.40	306.89	0.14	0.45	5.40	5.40	-7.62	1.37	0.49
	S_1	335.28	0.33	0.90	3.85	307.18	0.38	0.86	3.89	3.87	-13.05	1.75	0.37

polarization angle from the Rh(111) surface derives a relatively higher intensity than the high-energy bulk component, consistent with other observations.⁷⁻¹¹

Fig. 2 and 3 showed the measured $3d_{5/2}$ spectra from the (111), (100) and (110) planes of clean Pd and Rh surfaces. The Pd $3d_{5/2}$ spectra demonstrate one major peak that is symmetrical after background subtraction. However, the Rh $3d_{5/2}$ spectra exhibit two major peaks. The asymmetry at the lower energy end may correspond to the presence of defects in comparison to those of Pd. The XPS spectral pattern difference between Pd and Rh may arise from the electronic configurations Pd ($4d^{10}$) and Rh ($5s^1 4d^8$).

In order to conduct decomposition, all the spectra were normalized by their corresponding maximum intensity. According to the constraints given, each spectrum was decomposed with three components, representing the B, S_2 , and S_1 components from higher to lower BE. The decomposition was conducted by choosing $z_1 = 4$ for the (100) top layer^{7,11,38} as the standard and the z values for the rest components were optimized together with the fine tuning of the peaks of the components. The optimal component energies, the intensities, and the corresponding z_i values of the XPS $3d_{5/2}$ data for Rh and Pd surfaces after the subtraction of the Tougaard background are summarized in Table 1. Including the B component, there are a total of 7 components for the three surfaces of each specimen. The $\langle E_{3d}(0) \rangle$ should take the mean of the $C_7^2 = 7! / [(7-2)!] = 21 E_{3d}(0)$ values with a standard deviation σ . The refinement of the orientation-resolved effective CNs arises from the atomic density of each face. Results show the anisotropy of lattice strain and quantum trap depth in the three orientations due to the effective CNs.

From the decomposition, we obtained the $E_\nu(0)$ and $\Delta E_\nu(i)$ values. Generally, the intensity of the B component is higher than other components in the same spectrum and that the intensity of the B component is the highest in the (111) surface of the same material under the same experimental conditions. It has been shown that the BE for an isolated Rh atom is 302.163 ± 0.003 eV and for a Pd atom it is 330.261 ± 0.004 eV

with their respective bulk shifts of 4.367 and 4.359 eV. The asymmetric tails at the lower end of the Rh spectra suggest the presence of defects such as adatoms to the Rh surfaces. The refinement leads to the effective atomic CNs of the top (100), (110), and (111) atomic layers as 4.00, 3.87, and 4.26 and the CNs for the corresponding second layer as 5.73, 5.40 and 6.31. Results indicate that the BE of electrons in the top layer is in general the strongest, compared to electrons in the inner layers, which agrees with that discovered by Matsui *et al.*⁴⁰ on a Ni surface. Among the three surfaces, the electronic BE of the (110) surface is stronger than the (100) and the (111) surface because of their difference in the effective CNs. The findings in the current work lead to an expression for the z -resolved $3d_{5/2}$ core level shift for Rh and Pd:

$$E_\nu(i) = \langle E_{3d}(0) \rangle (\pm\sigma) + \Delta E_{3d}(B) c_z^{-1} \text{ (eV)}$$

$$= \begin{cases} 302.163(\pm 0.003) + 4.367 c_z^{-1} & \text{(Rh } 3d_{5/2}) \\ 330.261(\pm 0.004) + 4.359 c_z^{-1} & \text{(Pd } 3d_{5/2}) \end{cases} \text{ (eV)}$$

This fundamental information should be useful to the understanding of the behavior of these surfaces, such as their catalytic performance.

IV. Conclusion

We have applied the BOLS algorithm to the well-measured sets of orientation-resolved $3d_{5/2}$ core level shift of Pd and Rh surfaces. This combination has led to the following:

1. Establishment of constraints for decomposing an XPS spectrum in terms of the number, the order, and separation between the components. A positive core level shift due to the under-coordinated surface atoms has been further confirmed. The spectrum can be decomposed with components of B, S_2 , S_1 , and S_{defect} .

2. Extraction of quantitative information regarding the energy levels of an isolated atom and its bulk shift from the measured spectra. With the aid of XPS, we are able to gain

information about the local strain, quantum trap depth, binding energy density and atomic cohesive energy at an atomic site in the surface skins, which evidences the advantage of the combination of XPS and the BOLS approach and enhances the power of XPS.

3. It is further confirmed that the shorter and stronger bonds between under-coordinated atoms cause local strain and skin-depth charge and energy quantum trapping, and hence the global positive core level shifts that occur in other situations where under-coordinated atoms dominate.

The approach developed may provide an effective yet simple way of gaining information from XPS measurement and provides a consistent understanding of the core level shift induced by atomic CN reduction such as local sites around the original atomic defects, adatoms, surfaces, grain boundaries, dislocations, terrace edges, dimers, atomic chains, atomic sheets, hollow tubes, or the skin depth of nanostructures and nanocavities.

Acknowledgements

Financial support from Nanyang Technological University and the Agency for Science, Technology and Research, Singapore, the Nature Science Foundation (No. 10772157) of China, the Shanghai Natural Science Foundation (No. 07ZR14033), the Shanghai Pujiang Program (No. 08PJ14043), the Special Project for Nanotechnology of Shanghai (No. 0752nm011), and the Applied Materials Shanghai Research & Development Fund (No. 07SA12) are all gratefully acknowledged.

References

- 1 C. Q. Sun, *Prog. Mater. Sci.*, 2003, **48**, 521–685.
- 2 M. A. Omar, *Elementary Solid State Physics: Principles and Applications*, Addison-Wesley, New York, 1993.
- 3 C. Q. Sun, *Prog. Mater. Sci.*, 2009, **54**, 179–307.
- 4 A. Zangwill, *Physics At Surfaces*, Cambridge University Press, 1988.
- 5 C. Q. Sun, *Phys. Rev. B: Condens. Matter Mater. Phys.*, 2004, **69**, 045105.
- 6 W. D. Phillips, *Rev. Mod. Phys.*, 1998, **70**, 721–741.
- 7 B. S. Fang, W. S. Lo, T. S. Chien, T. C. Leung, C. Y. Lue, C. T. Chan and K. M. Ho, *Phys. Rev. B: Condens. Matter*, 1994, **50**, 11093–11101.
- 8 M. Alden, H. L. Skriver and B. Johansson, *Phys. Rev. Lett.*, 1993, **71**, 2449–2452.
- 9 B. Balamurugan and T. Maruyama, *Appl. Phys. Lett.*, 2006, **89**, 033112.
- 10 E. Navas, K. Starke, C. Laubschat, E. Weschke and G. Kaindl, *Phys. Rev. B: Condens. Matter*, 1993, **48**, 14753–14755.
- 11 R. A. Bartynski, D. Heskett, K. Garrison, G. Watson, D. M. Zehner, W. N. Mei, S. Y. Tong and X. Pan, *J. Vac. Sci. Technol., A*, 1989, **7**, 1931–1936.
- 12 J. N. Andersen, D. Hennig, E. Lundgren, M. Methfessel, R. Nyholm and M. Scheffler, *Phys. Rev. B: Condens. Matter*, 1994, **50**, 17525–17533.
- 13 D. M. Riffe and G. K. Wertheim, *Phys. Rev. B: Condens. Matter*, 1993, **47**, 6672–6679.
- 14 J. H. Cho, K. S. Kim, S. H. Lee, M. H. Kang and Z. Y. Zhang, *Phys. Rev. B: Condens. Matter Mater. Phys.*, 2000, **61**, 9975–9978.
- 15 A. V. Fedorov, E. Arenholz, K. Starke, E. Navas, L. Baumgarten, C. Laubschat and G. Kaindl, *Phys. Rev. Lett.*, 1994, **73**, 601–604.
- 16 L. I. Johansson, H. I. P. Johansson, J. N. Andersen, E. Lundgren and R. Nyholm, *Phys. Rev. Lett.*, 1993, **71**, 2453–2456.
- 17 Y. Sun, J. S. Pan, J. G. Tao, Y. G. Nie, C. H. A. Huan, Z. Zhang, J. W. Chai, D. Li, S. J. Wang and C. Q. Sun, *J. Phys. Chem. C*, 2009, **113**, 10939–10946.
- 18 J. G. Tao, J. S. Pan, C. H. A. Huan, Z. Zhang, Y. Sun, J. W. Chai and S. J. Wang, *J. Phys.: Condens. Matter*, 2008, **20**, 485002.
- 19 T. H. Lin, T. P. Huang, Y. L. Liu, C. C. Yeh, Y. H. Lai and W. H. Hung, *Surf. Sci.*, 2005, **578**, 27–34.
- 20 Y. Sun, Y. Wang, J. S. Pan, L. L. Wang and C. Q. Sun, *J. Phys. Chem. C*, 2009, **113**, 14696–14701.
- 21 J. F. Zhu, M. Kinne, T. Fuhrmann, R. Denecke and H. P. Steinruck, *Surf. Sci.*, 2003, **529**, 384–396.
- 22 D. Q. Yang and E. Sacher, *Chem. Mater.*, 2006, **18**, 1811–1816.
- 23 L. Bianchettin, A. Baraldi, S. de Gironcoli, E. Vesselli, S. Lizzit, L. Petaccia, G. Comelli and R. Rosei, *J. Chem. Phys.*, 2008, **128**, 114706.
- 24 P. Marcus and C. Hinnen, *Surf. Sci.*, 1997, **392**, 134–142.
- 25 D. Q. Yang and E. Sacher, *J. Phys. Chem. C*, 2008, **112**, 4075–4082.
- 26 C. Bittencourt, M. Hecq, A. Felten, J. J. Pireaux, J. Ghijsen, M. P. Felicissimo, P. Rudolf, W. Drube, X. Ke and G. Van Tendeloo, *Chem. Phys. Lett.*, 2008, **462**, 260–264.
- 27 T. Ohgi and D. Fujita, *Phys. Rev. B: Condens. Matter Mater. Phys.*, 2002, **66**, 115410.
- 28 A. Howard, D. N. S. Clark, C. E. J. Mitchell, R. G. Egdell and V. R. Dhanak, *Surf. Sci.*, 2002, **518**, 210–224.
- 29 M. Salmeron, S. Ferrer, M. Jazzar and G. A. Somorjai, *Phys. Rev. B: Condens. Matter*, 1983, **28**, 1158–1160.
- 30 D. Q. Yang and E. Sacher, *Appl. Surf. Sci.*, 2002, **195**, 187–195.
- 31 C. N. R. Rao, G. U. Kulkarni, P. J. Thomas and P. P. Edwards, *Chem.–Eur. J.*, 2002, **8**, 29–35.
- 32 C. Q. Sun, L. K. Pan, Y. Q. Fu, B. K. Tay and S. Li, *J. Phys. Chem. B*, 2003, **107**, 5113–5115.
- 33 C. Q. Sun, Y. Sun, Y. G. Nie, Y. Wang, J. S. Pan, G. Ouyang, L. K. Pan and Z. Sun, *J. Phys. Chem. C*, 2009, **113**, 16464–16467.
- 34 H. Hibino, H. Kageshima, M. Kotsugi, F. Maeda, F.-Z. Guo and Y. Watanabe, *Phys. Rev. B: Condens. Matter Mater. Phys.*, 2009, **79**, 125437.
- 35 K. J. Kim, H. Lee, J. H. Choi, Y. S. Youn, J. Choi, T. H. Kang, M. C. Jung, H. J. Shin, H. J. Lee, S. Kim and B. Kim, *Adv. Mater.*, 2008, **20**, 3589.
- 36 J. Nanda and D. D. Sarma, *J. Appl. Phys.*, 2001, **90**, 2504–2510.
- 37 X. J. Liu, J. W. Li, Z. F. Zhou, L. W. Yang, Z. S. Ma, G. F. Xie, Y. Pan and C. Q. Sun, *Appl. Phys. Lett.*, 2009, **94**, 131902.
- 38 C. Q. Sun, *Prog. Solid State Chem.*, 2007, **35**, 1–159.
- 39 A. Baraldi, L. Bianchettin, E. Vesselli, S. de Gironcoli, S. Lizzit, L. Petaccia, G. Zampieri, G. Comelli and R. Rosei, *New J. Phys.*, 2007, **9**(143), 12.
- 40 F. Matsui, T. Matsushita, Y. Kato, M. Hashimoto, K. Inaji, F. Z. Guo and H. Daimon, *Phys. Rev. Lett.*, 2008, **100**, 207201.
- 41 W. J. Huang, R. Sun, J. Tao, L. D. Menard, R. G. Nuzzo and J. M. Zuo, *Nat. Mater.*, 2008, **7**, 308–313.
- 42 W. H. Qi, H. B. Y. and W. M. P., *J. Adhes. Sci. Technol.*, 2009, **6**, 635–639.